Supplement S1 - Model optimization

The 6 parameters controlling $Vcmax$, θg and S (Table 1), influencing the GPP values for black spruce, were optimized within a Bayesian framework using observed data at EOBS as reference and Markov Chain Monte Carlo (MCMC) sampling with Metropolis-Hastings steps. The MCMC sampling, through its iterations, only retained the combinations of parameters satisfying the following condition:

$$P_y < e^{(L_y - L_{y-1})};\ L_y = \prod_{i=1}^{nobs} N(Obs_i;\ \mu = Sim_i, \sigma_y)\, p(\psi_y) \quad \text{(S1)}$$

In Eq. (S1), P_y is a random number between 0 and 1 picked-up at iteration y and L_y is the model posterior probability computed with the product between the model likelihood ($\prod_{i=1}^{nobs} N(Obs_i;\ \mu = Sim_i, \sigma_y)$) and the parameter priors ($p(\psi_y)$). Here we assumed that the model likelihood can be calculated using normal probability densities where Obs_i is an observed GPP daily value, Sim_i is its simulated equivalent and σ_y is the standard deviation of deviations between observation and simulation at iteration y. Moreover, ψ_y is the hyperparameter vector at iteration y composed of the 6 parameters to be optimized plus σ_y. The prior for the 6 parameters was supposed to be uniform over an acceptable range (Table 1), while a Jeffreys prior was used for σ ($\propto 1/\sigma$). In this way, the MCMC sampling maximizes the model posterior probability according to model possibility (i.e. the ability of the model to approximate plausible GPP daily values).

The 12 parameters strongly influencing the MAIDEN Dstem for black spruce (Table 1) were optimized similarly to those 6 influencing GPP. In the computation of the model likelihood (Eq. (S1)), Obs_i was an observed RWhighF value and Sim_i was a simulated detrended yearly Dstem (similarly to RWhighF the detrending was achieved by subtraction by a 10-year cubic smoothing spline). To allow the comparison, both *Obs* and *Sim* were transformed to z-scores. We preferred to optimize MAIDEN on RWhighF values because tree-ring high frequencies are much more robust regionally across sites and trees than low frequencies. Observed and simulated low frequencies were only compared after the optimization of the model parameters.

In the calibration process, to verify the convergence of the sampling, we ran 50 Markov chains starting each time from random initial conditions (i.e. initial values of the parameters in their acceptable ranges). Finally, for each chain, we only selected the iteration with higher model posterior probability. In this way, we got 50 blocks of potential parameters. The convergence of the sampling is shown by the sharp parameters' posterior densities (Figs. S4 and S8) and by the stabilization of the model posterior probability in the 50 chains (Fig. S1). The acceptable ranges (i.e. biologically sound) in which the parameters were sampled are shown in Table 1.

The MAIDENiso GPP is determined by the 6 calibrated parameters (Table 1), but is also influenced by variations in the canopy biomass, which, in part, depend on the values of the parameters controlling the carbon allocation. To avoid that the parameter selection during the MCMC sampling used to calibrate the MAIDENiso GPP was sensitive to the values of the parameters controlling the carbon allocation, we calibrated the 6 GPP parameters fixing the carbon contained in the canopy

reservoir at a constant value. Subsequently, during the calibration of the parameters controlling the carbon allocation, the carbon in the canopy was allowed to vary. In this way, the GPP calibration is independent from the calibration of the carbon allocation, but the parameter selection for the allocation depends on the GPP parameters.

For both the GPP and the carbon allocation, we selected a block of parameters that we called "Plausible Block" ("Plausible Block GPP" and "Plausible Block Stem") and often used to illustrate the results. The selection was based on these criteria:

$$\left(L_y > L_{mode}\right) \,\&\, \left(\sum_{z=1}^{n}\left(ParL_{\psi_{y,z}} \cdot ParRange_z\right) = Maximum\right) \rightarrow \left(\psi_y = Plausible\ Block\right) \quad \text{(S2)}$$

Basically, the model posterior probability with this block of parameters (L_y) must be higher than the mode of the 50 retained iterations (Fig. S1) and the sum of the products between the parameters' posterior probabilities ($ParL$; Figs. S4 and S8) and the spans of their acceptable ranges ($ParRange$) must be maximized. ψ_y is the hyperparameter vector at iteration y (here not including σ_y) composed of n parameters. The reader should note that the two Plausible Blocks are only a possibility over the retained iterations, which were used to simplify visualizations and interpretations.

The robustness of the parameters' posterior distributions was tested with a cross-validation exercise. Firstly, we compared the parameters' posterior densities, when the optimization was executed on the full period with observed data, to those obtained with half data (Figs. S5 and S9). However, we have to recall that in total we have 2920 observed daily data between 2003 and 2010 to optimize the 6 parameters influencing the GPP, and only 61 observed ring width annual data between 1950 and 2010 to optimize the 12 parameters influencing Dstem. Subsequently, the distributions of the parameters influencing Dstem were also compared to those obtained independently with data from specific sites (the used black spruce ring width data comes from five different riparian forests; Fig. S10).

Supplement S2 – Data provenance and treatment

Eddy covariance stations provide measurements of net ecosystem production (NEP), as well as estimates of gross ecosystem production (GEP) and respiration (R) for specific sites. There is one eddy covariance station from the Fluxnet network located in a mature black spruce forest in the northern Quebec taiga. It is the "Quebec Eastern Old Black Spruce" station (EOBS; 49.69N and 74.34W; Bergeron et al., 2007; http://fluxnet.ornl.gov/site/269) with data from 2003 to 2010. Although NEP and R from eddy covariance stations are not directly comparable with MAIDEN outputs because they integrate all ecosystem components (e.g. soil heterotrophic respiration), GEP was assumed to be comparable to the simulated GPP, because GEP only derives from the autotrophic components of the ecosystem (Gea-Izquierdo et al., 2014). Consequently, we integrated the GEP half-hourly time series from the EOBS site in a daily time series (Fig. S2), to make it comparable with the MAIDEN GPP for the same location. We then used these data to optimize the six parameters influencing the stand GPP simulated by the model for black spruce forests. In the paper, we employ the term GPP also to denote GEP estimates from the EOBS site.

We assumed that the yearly Dstem is proportional to tree-ring growth in order to use ring width data to optimize MAIDEN (12 influential parameters). We used data from 46 black spruce trees sampled in the riparian forests of five lakes in the eastern Canadian taiga (Gennaretti et al., 2014; the coordinates of the central point are 54.26N and 71.34W). The time series (Fig. S3; Dataset S1) were standardized using a site-specific Regional Curve Standardization (Gennaretti et al., 2014) and averaged to obtain a regional chronology (hereafter RW) to compare with MAIDEN annual stem carbon increments (g $C \cdot m^{-2}$ of $stand \cdot year^{-1}$). However, because we wanted to analyze both the multi-decadal and the inter-annual variability of carbon allocation, we subsequently detrended all standardized ring width time series by subtracting their respective 10-year cubic smoothing splines (50% frequency cutoff for 10-year periods). The resulting detrended regional chronology (hereafter RWhighF) was compared with MAIDEN annual stem carbon increments, detrended in the same way. RWhighF was also used as a reference for the optimization of the MAIDEN parameters (Supplement S1). We preferred to optimize MAIDEN on RWhighF values because tree-ring high frequencies are much more robust regionally across sites and trees than low frequencies. Observed and simulated low frequencies were only compared after the optimization of the model parameters. MAIDEN outputs were simulated for the central point of the source area of ring width data over the 1950-2010 period. Such a spatial aggregation of tree-ring data is known to reduce non-climatic noise at the site level, thus increasing the coherence between modeled and observed time series (Breitenmoser et al., 2014).

MAIDEN needs daily climate data as inputs. These data were obtained from the gridded interpolated Canadian database of daily minimum–maximum temperature and precipitation for 1950-2015 (Hutchinson et al., 2009; http://cfs.nrcan.gc.ca/projects/3/4). We extracted the time series from the grid cells nearest to the studied locations (the eddy covariance station and the central point of the region with collected ring width data). CO_2 atmospheric concentration values for the same sites were obtained from the nearest grid cell of the CarbonTracker measurement and modeling system (2000-2015 period; Peters et al., 2007; http://www.esrl.noaa.gov/gmd/ccgg/carbontracker/). In order to obtain longer CO_2 time series (1950–2015), the seasonal cycle from the selected cells of the CarbonTracker grid was superimposed to the long-term CO_2 trend from the Mauna Loa observatory (1958-2015; Keeling et al., 1976; http://www.esrl.noaa.gov/gmd/ccgg/trends/) with removed seasonal cycle, extrapolated before 1958, and modified by adding the mean offset between the selected cells and the Mauna Loa cell in the CarbonTracker grid.

Bergeron, O., Margolis, H. A., Black, T. A., Coursolle, C., Dunn, A. L., Barr, A. G., and Wofsy, S. C.: Comparison of carbon dioxide fluxes over three boreal black spruce forests in Canada, Glob. Change Biol., 13, 89-107, doi:10.1111/j.1365-2486.2006.01281.x, 2007.

Breitenmoser, P., Brönnimann, S., and Frank, D.: Forward modelling of tree-ring width and comparison with a global network of tree-ring chronologies, Clim. Past, 10, 437-449, doi:10.5194/cp-10-437-2014, 2014.

Gea-Izquierdo, G., Bergeron, Y., Huang, J. G., Lapointe-Garant, M. P., Grace, J., and Berninger, F.: The relationship between productivity and tree-ring growth in boreal coniferous forests, Boreal Environ. Res., 19, 363-378, 2014.

Gennaretti, F., Arseneault, D., Nicault, A., Perreault, L., and Bégin, Y.: Volcano-induced regime shifts in millennial tree-ring chronologies from northeastern North America, P. Natl. Acad. Sci. USA, 111, 10077-10082, doi:10.1073/pnas.1324220111, 2014.

Hutchinson, M. F., McKenney, D. W., Lawrence, K., Pedlar, J. H., Hopkinson, R. F., Milewska, E., and Papadopol, P.: Development and testing of Canada-wide interpolated spatial models of daily minimum-maximum temperature and precipitation for 1961-2003, J. Appl. Meteorol. Clim., 48, 725-741, doi:10.1175/2008jamc1979.1, 2009.

Keeling, C. D., Bacastow, R. B., Bainbridge, A. E., Ekdahl, C. A., Guenther, P. R., Waterman, L. S., and Chin, J. F. S.: Atmospheric carbon dioxide variations at Mauna Loa Observatory, Hawaii, Tellus, 28, 538-551, doi:10.1111/j.2153-3490.1976.tb00701.x, 1976.

Peters, W., Jacobson, A. R., Sweeney, C., Andrews, A. E., Conway, T. J., Masarie, K., Miller, J. B., Bruhwiler, L. M. P., Pétron, G., Hirsch, A. I., Worthy, D. E. J., van der Werf, G. R., Randerson, J. T., Wennberg, P. O., Krol, M. C., and Tans, P. P.: An atmospheric perspective on North American carbon dioxide exchange: CarbonTracker, P. Natl. Acad. Sci. USA, 104, 18925-18930, doi:10.1073/pnas.0708986104, 2007.

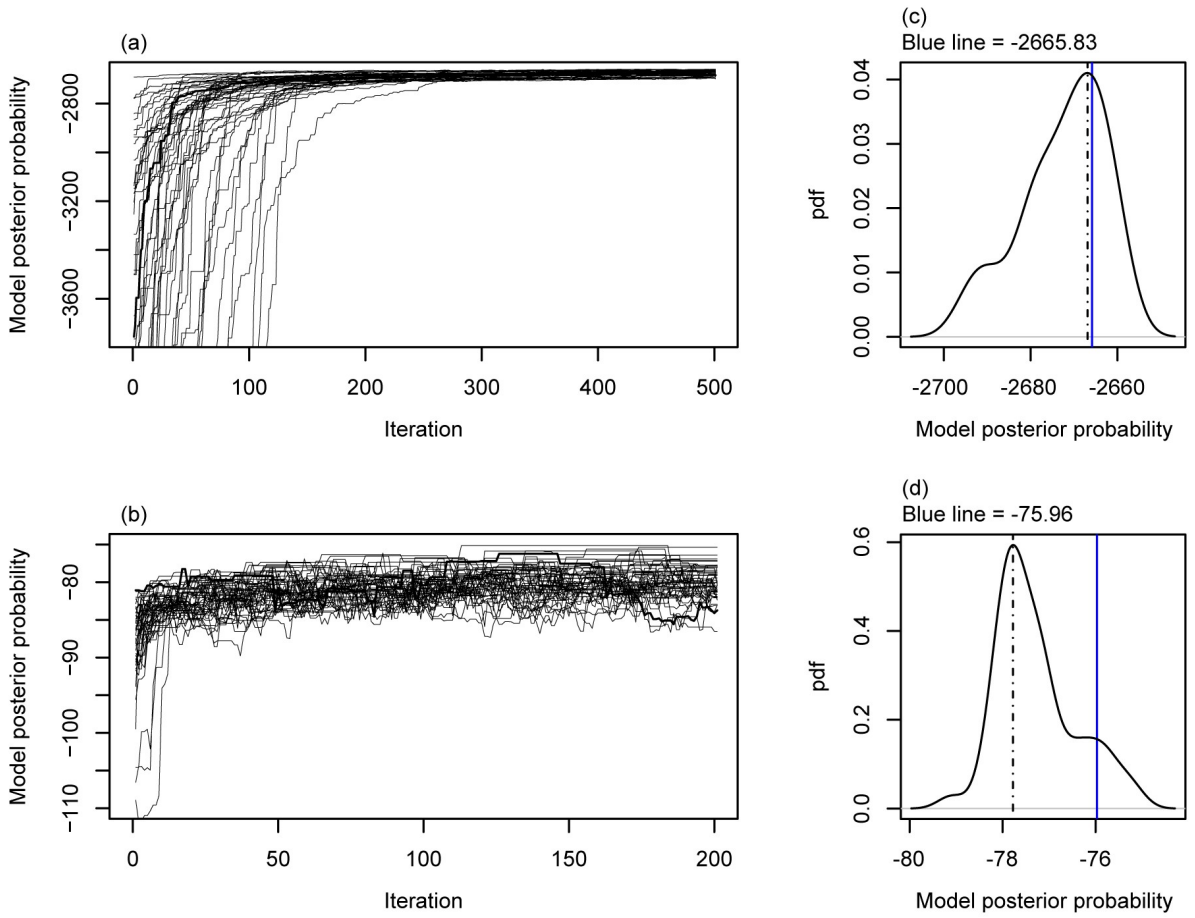

Figure S1: Evolution of the model posterior probability in the 50 Markov chains used in the MAIDENiso calibration. (a) Calibration of GPP (i.e. 6 parameters). (b) Calibration of carbon allocation to the stem (i.e. 12 parameters). Plots (c) and (d) show the model posterior density of the retained 50 blocks of parameters (one block per each chain of (a) and (b)). Vertical dashed line is the mode and blue line is the value with the respective Plausible Block.

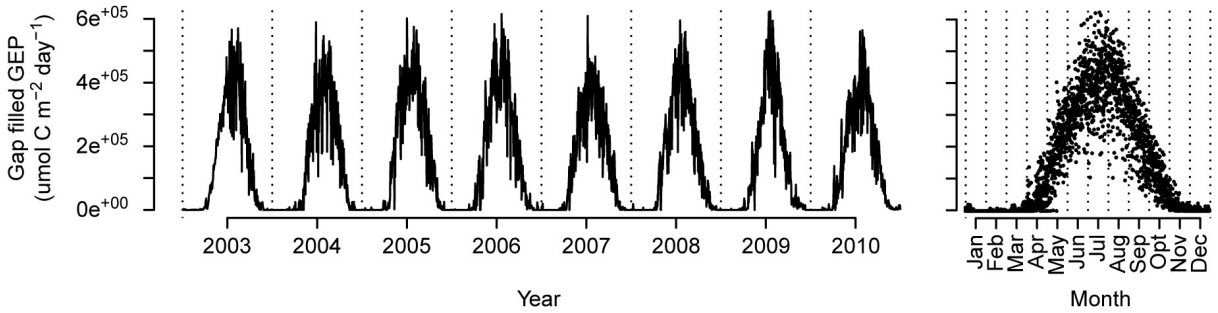

Figure S2: "Quebec Eastern Old Black Spruce" (EOBS) GPP gap filled daily time series (left) and annual cycle (right). 2003-2010 period. Units are umol C m^{-2} day^{-1}.

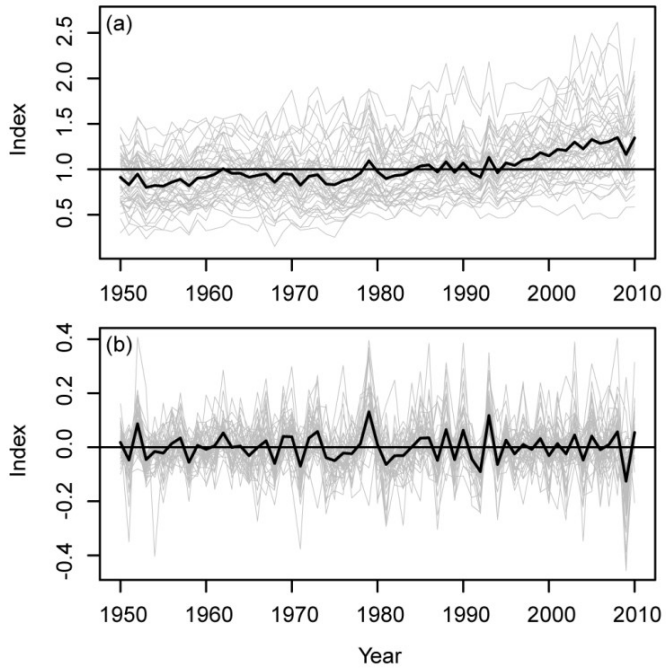

Figure S3: Time series of used ring width data. (a) Site-specific RCS standardized. (b) Site-specific RCS standardized and detrended. Individual series are in grey and the mean (corresponding to RW and RWhighF) is in black.

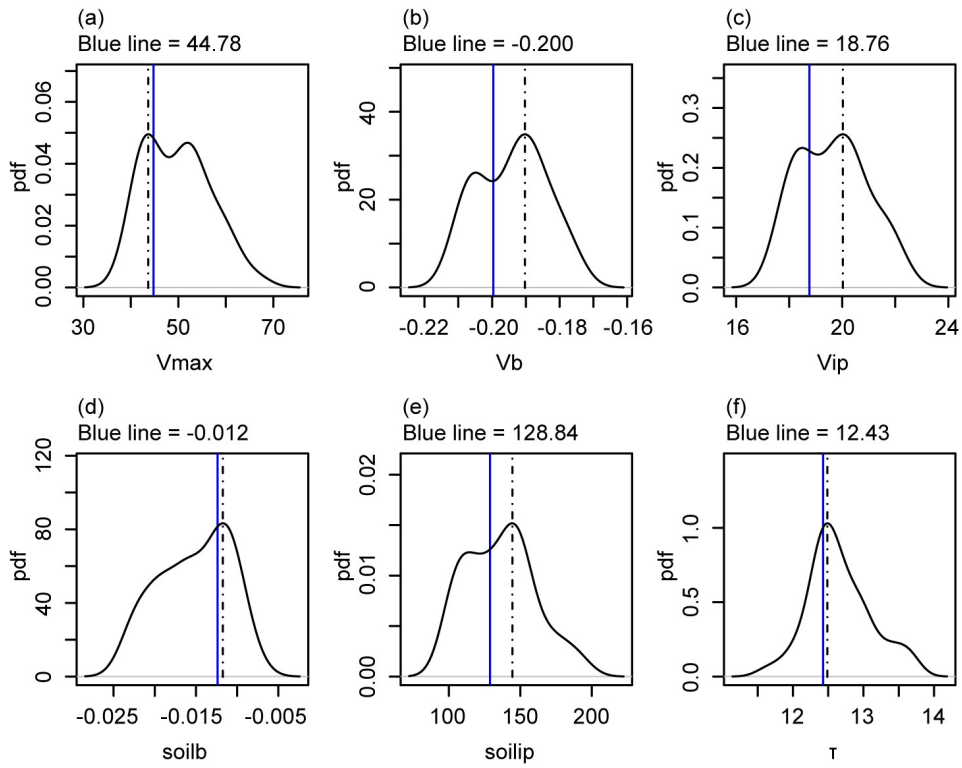

Figure S4: Parameters' posterior densities (pdfs based on 50 values). (a) *Vmax*, (b) *Vb*, (c) *Vip*, (d) *soilb*, (e) *soilip*, and (f) τ. Vertical dashed line is the mode and blue line is the value with Plausible Block GPP.

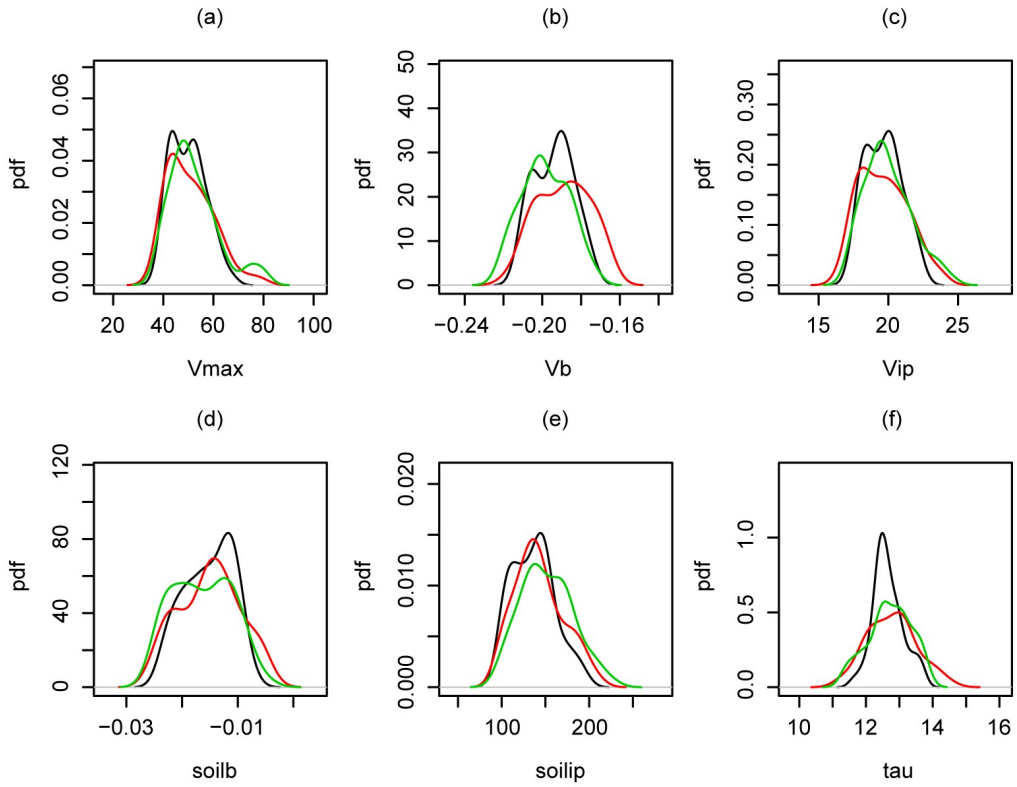

Figure S5: Cross-validation of parameters. Posterior densities (pdfs based on 50 values) of (a) *Vmax*, (b) *Vb*, (c) *Vip*, (d) *soilb*, (e) *soilip*, and (f) τ when parameters are optimized on the full period (black; using 2920 GPP observed daily data between 2003 and 2010), on the first half (red; using 1460 GPP observed daily data between 2003 and 2006) or on the second half (green; using 1460 GPP observed daily data between 2007 and 2010).

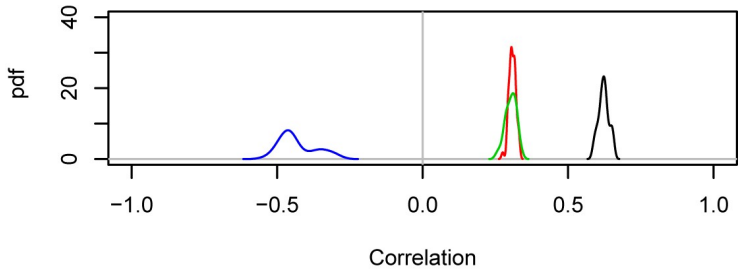

Figure S6: Correlation between the mean of the detrended series of black spruce ring growth (RWhighF) and simulated yearly detrended C allocation to the stem (black) or GPP annual values (red: sum from January to December; green: sum from Phase 5 of the previous year to Phase 4; blue: sum from Phase 4 of the previous year to Phase 3; MAIDEN phases are illustrated in Fig. 1). The pdfs are based on the 50 simulations retained by the Bayesian optimization.

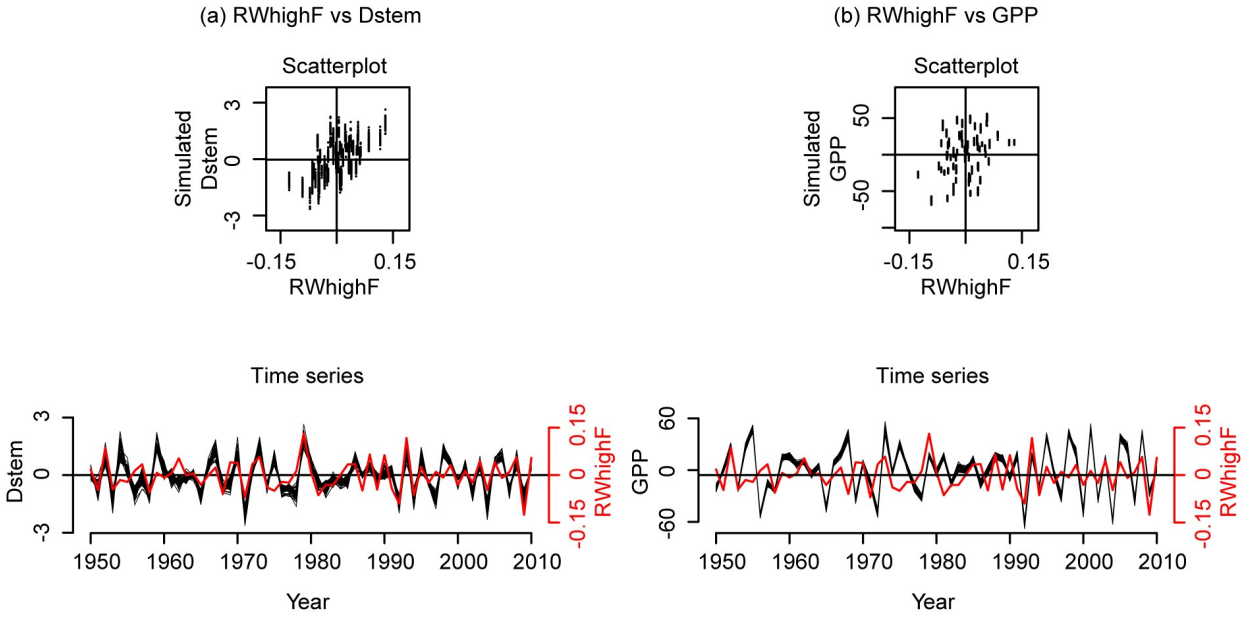

Figure S7: Comparison between the observed detrended mean series of black spruce ring growth (RWhighF) and MAIDEN simulated detrended carbon allocation to stem (plot a; g C m^{-2} $year^{-1}$; r=0.62, df=59, p<0.001), or simulated detrended GPP (plot b; g C m^{-2} $year^{-1}$; r=0.31, df=59, p<0.05). In all plots, observations are compared with the values from all iterations retained by the MCMC sampling.

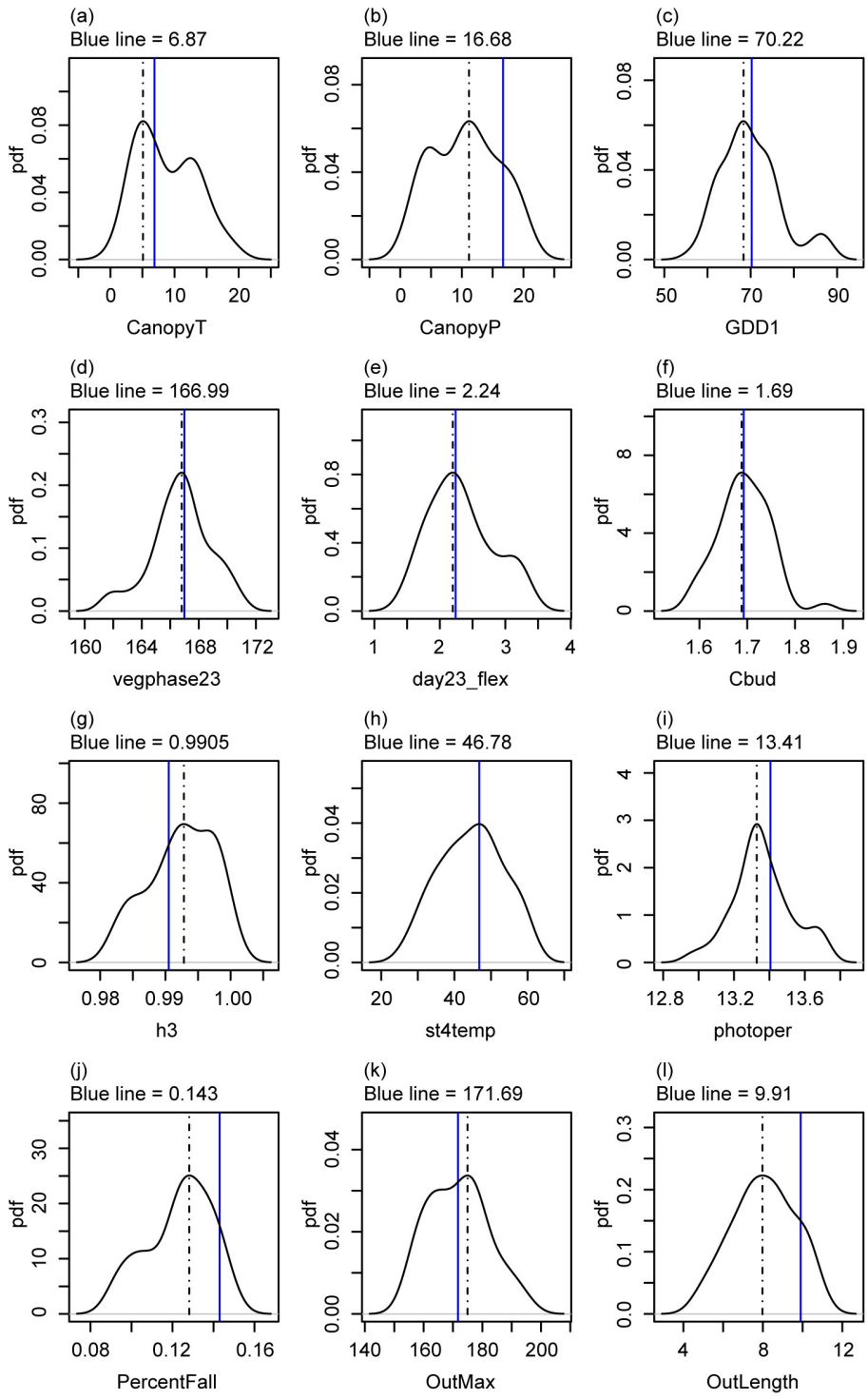

Figure S8: Parameters' posterior densities (pdfs based on 50 values). (a) *CanopyT*, (b) *CanopyP*, (c) *GDD1*, (d) *vegphase23*, *(e) day23_flex*, (f) *Cbud*, (g) *h3*, (h) *st4temp*, (i) *photoper*, (j) *PercentFall*, (k) *OutMax*, (l) *OutLength*. Vertical dashed line is the mode and blue line is the value with Plausible Block Stem.

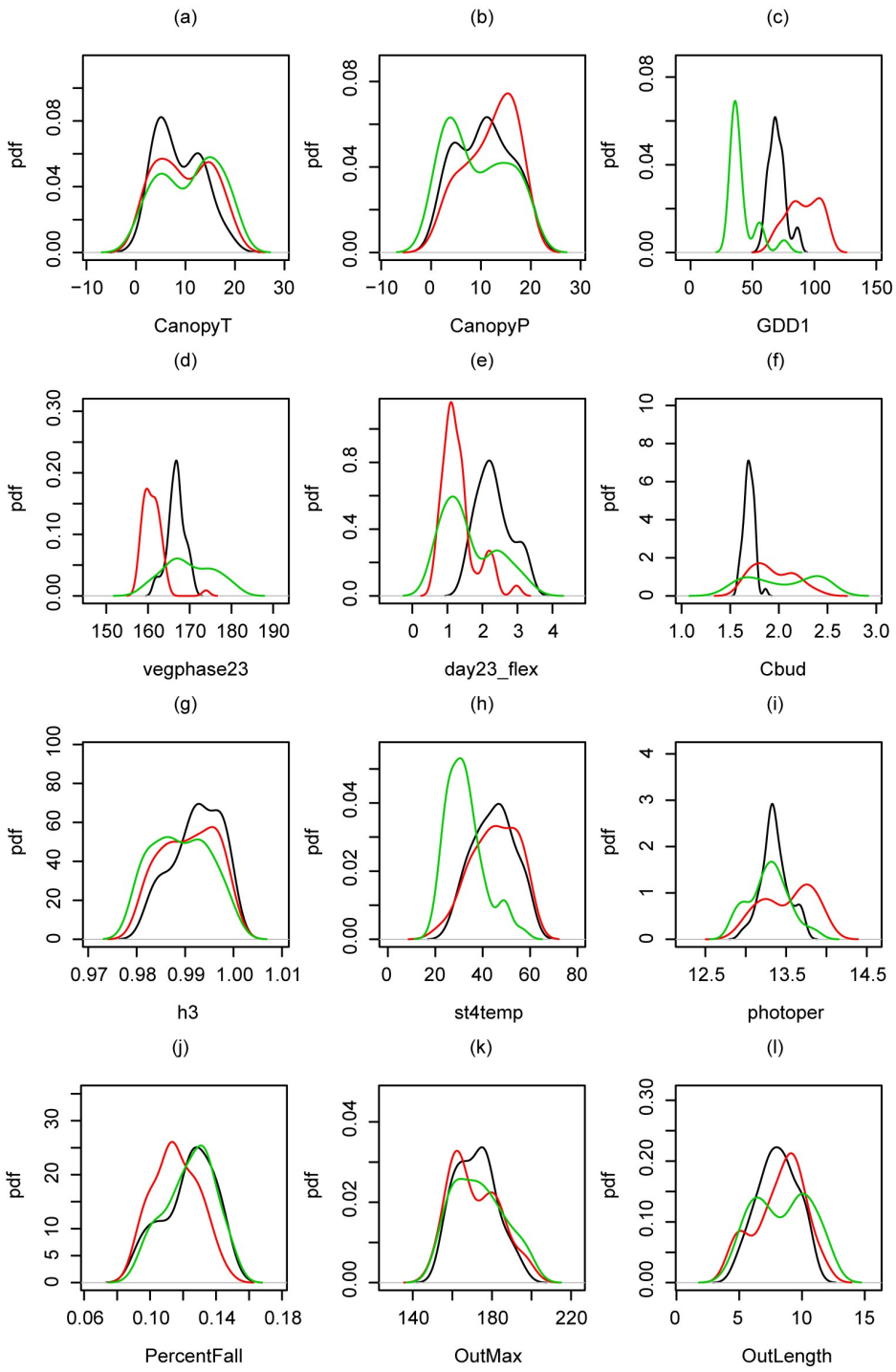

Figure S9: Cross-validation of parameters. Posterior densities (pdfs based on 50 values) of (a) *CanopyT*, (b) *CanopyP*, (c) *GDD1*, (d) *vegphase23*, *(e) day23_flex*, (f) *Cbud*, (g) *h3*, (h) *st4temp*, (i) *photoper*, (j) *PercentFall*, (k) *OutMax*, (l) *OutLength* when parameters are optimized on the full period (black; using 61 observed yearly RWhighF data between 1950 and 2010), on the first half (red; using 31 observed yearly RWhighF data between 1950 and 1980) or on the second half (green; using 30 observed yearly RWhighF data between 1981 and 2010).

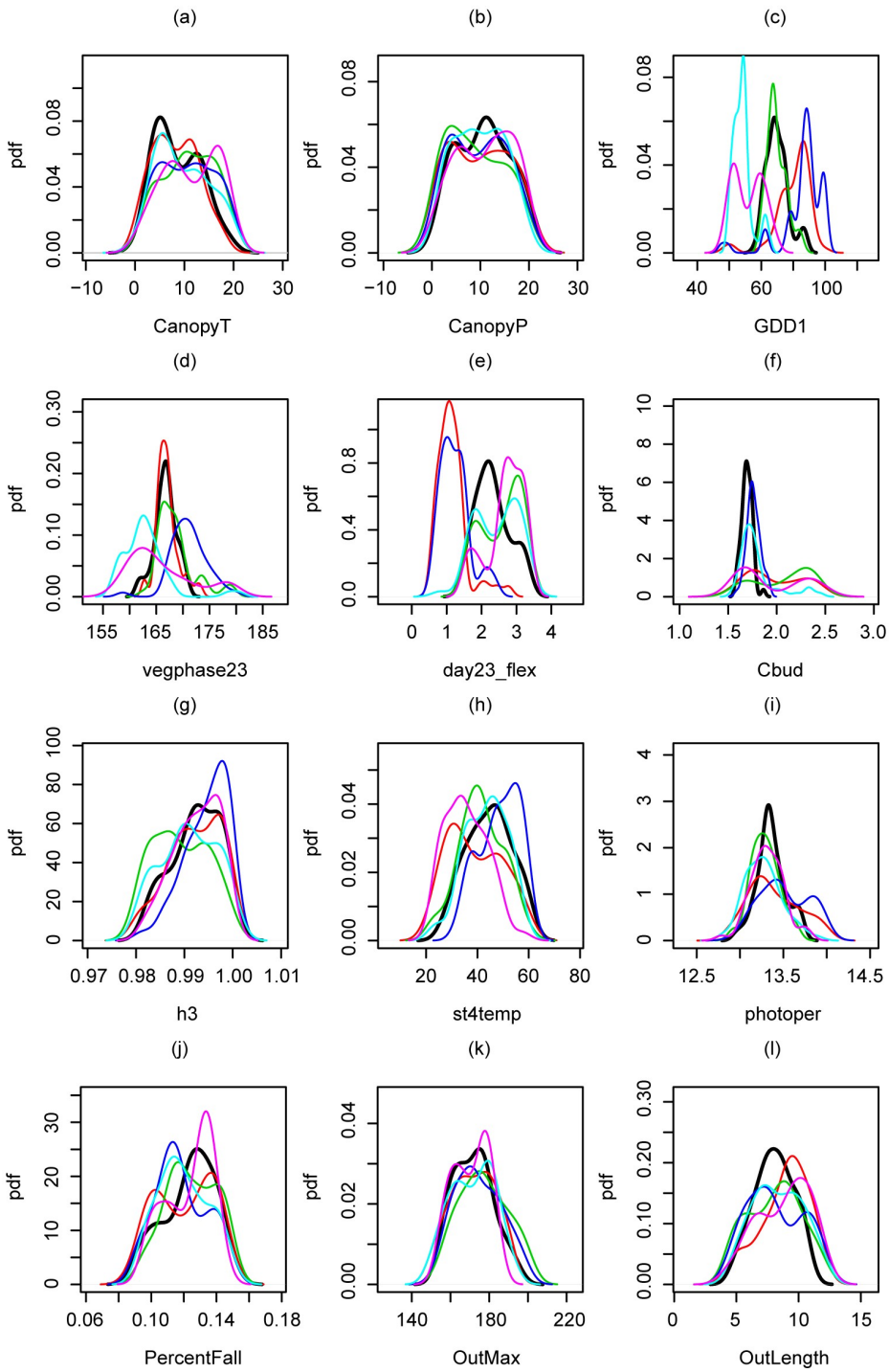

Figure S10: Cross-validation of parameters. Posterior densities (pdfs based on 50 values) of (a) *CanopyT*, (b) *CanopyP*, (c) *GDD1*, (d) *vegphase23*, *(e) day23_flex*, (f) *Cbud*, (g) *h3*, (h) *st4temp*, (i) *photoper*, (j) *PercentFall*, (k) *OutMax*, (l) *OutLength* when parameters are optimized on data from all sites (black; using 61 observed yearly RWhighF data between 1950 and 2010), or on data from specific sites (5 colored lines).

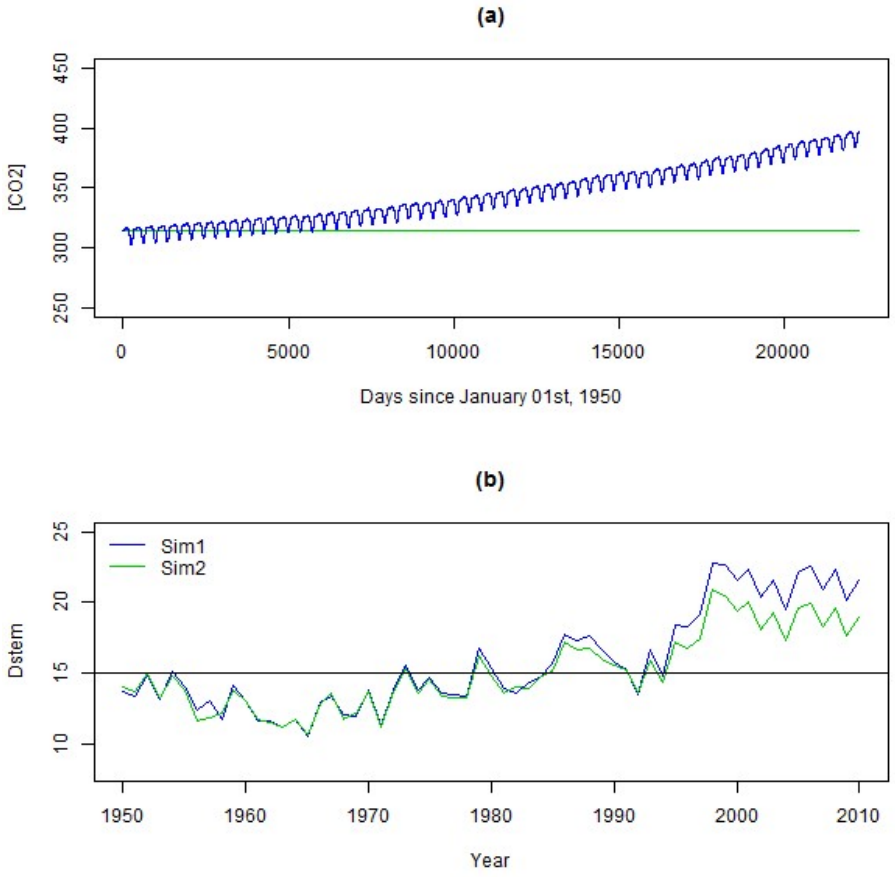

Figure S11: CO_2 impact on simulated Dstem. MAIDEN is run twice with the parameters of Plausible Block Stem at the center of the region with ring width data in the northern Quebec taiga. The first time (blue) we use plausible CO_2 values for the region (plot a; see Supplement S2) obtaining a Dstem time series (plot b; g C m^{-2} $year^{-1}$). The second time (green) we use constant CO_2 values.

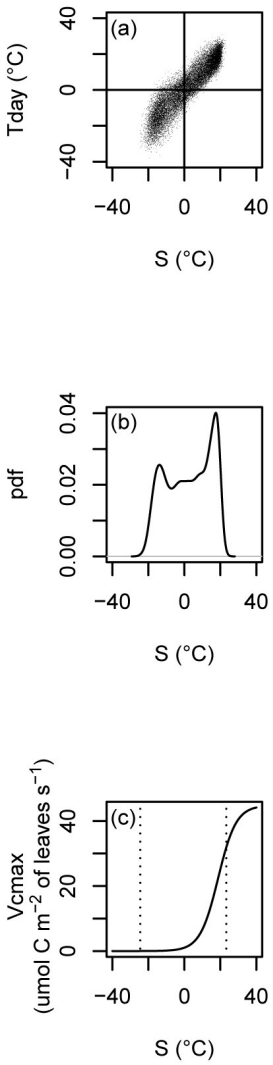

Figure S12: Temperature dependence of maximum carboxylation rate (*Vcmax*) when MAIDENiso is run with the parameters of Plausible Block GPP at the Quebec Eastern Old Black Spruce site (EOBS). (a) Relationship between daytime temperature ($Tday$) and its transformation used in the *Vcmax* equation (*S*). (b) *S* probability density at EOBS. (c) Relationship between *S* and *Vcmax*. The vertical dashed lines show the range of *S* values at EOBS.

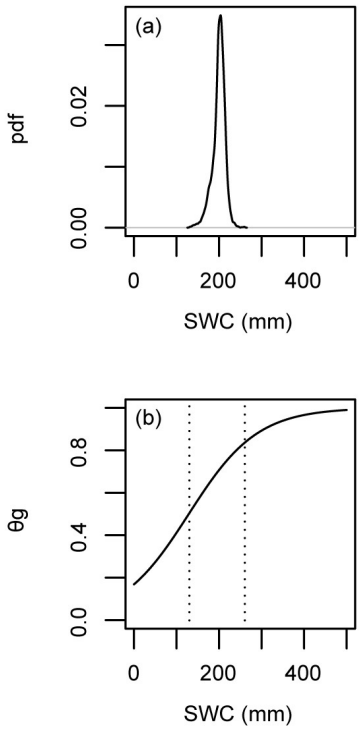

Figure S13: Water stress level (θg) function when MAIDENiso is run with the parameters of Plausible Block GPP at the Quebec Eastern Old Black Spruce site (EOBS). (a) Soil water content (*SWC*) probability density at EOBS. (b) Relationship between *SWC* and θg (higher values correspond to lower stress). The vertical dashed lines show the range of *SWC* values at EOBS.

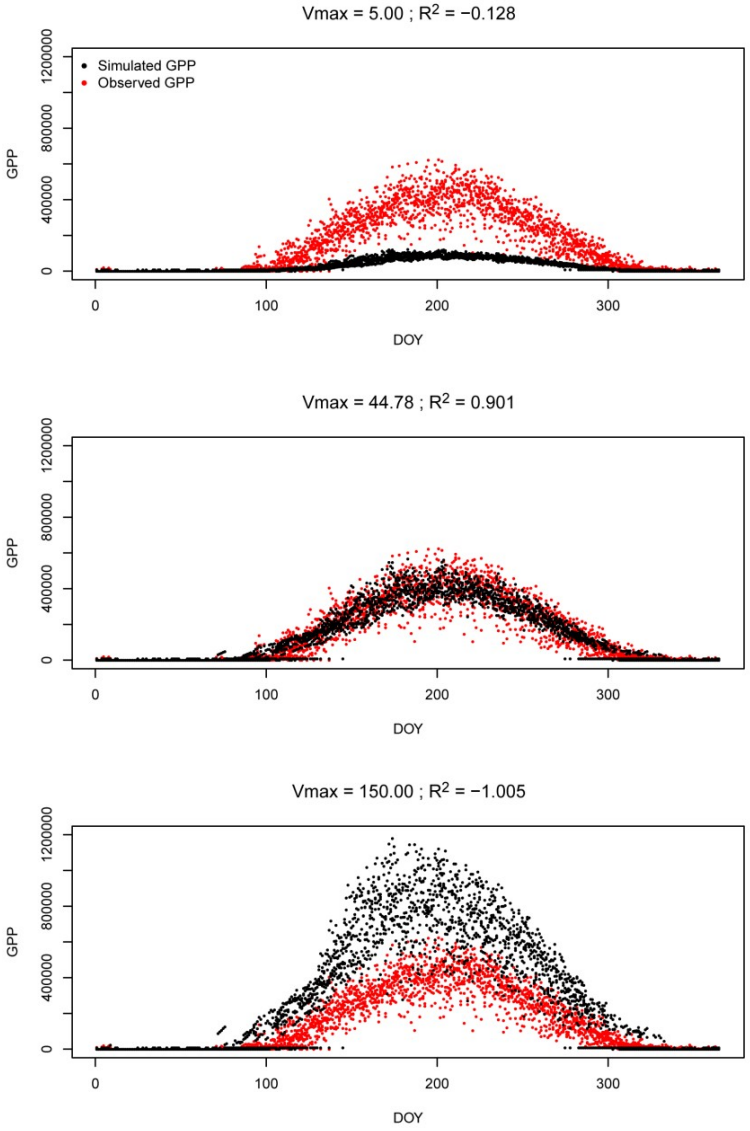

Figure S14: Sensitivity of the daily GPP simulated annual cycle (umol C m^{-2} day^{-1}) to the *Vmax* parameter influencing $Vcmax$. Only *Vmax* varies while the other parameters were fixed to the values of Plausible Block GPP. In the top (bottom) plot, *Vmax* was fixed to the lowest (highest) value of its prior acceptable range. In the middle plot, it was fixed to the selected value for Plausible Block GPP. The R^2 between observations and simulations and the parameter value are reported for each plot.

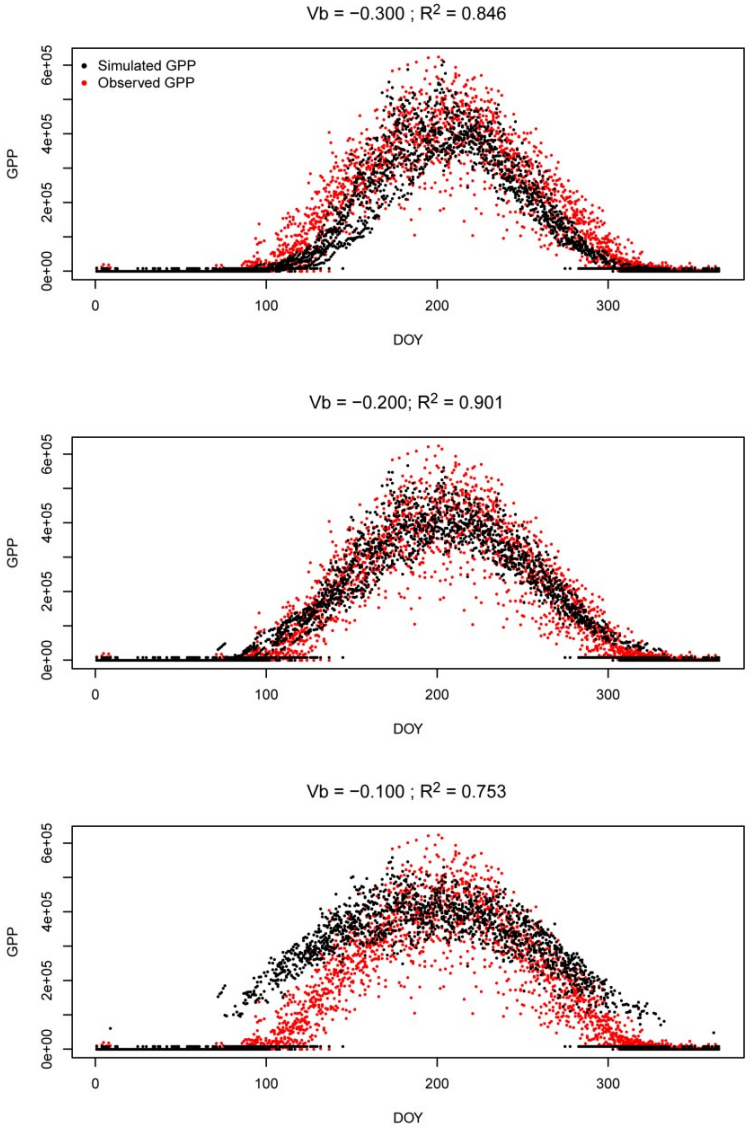

Figure S15: Sensitivity of the daily GPP simulated annual cycle (umol C m^{-2} day^{-1}) to the *Vb* parameter influencing $Vcmax$. Only *Vb* varies while the other parameters were fixed to the values of Plausible Block GPP. In the top (bottom) plot, *Vb* was fixed to the lowest (highest) value of its prior acceptable range. In the middle plot, it was fixed to the selected value for Plausible Block GPP. The R^2 between observations and simulations and the parameter value are reported for each plot.

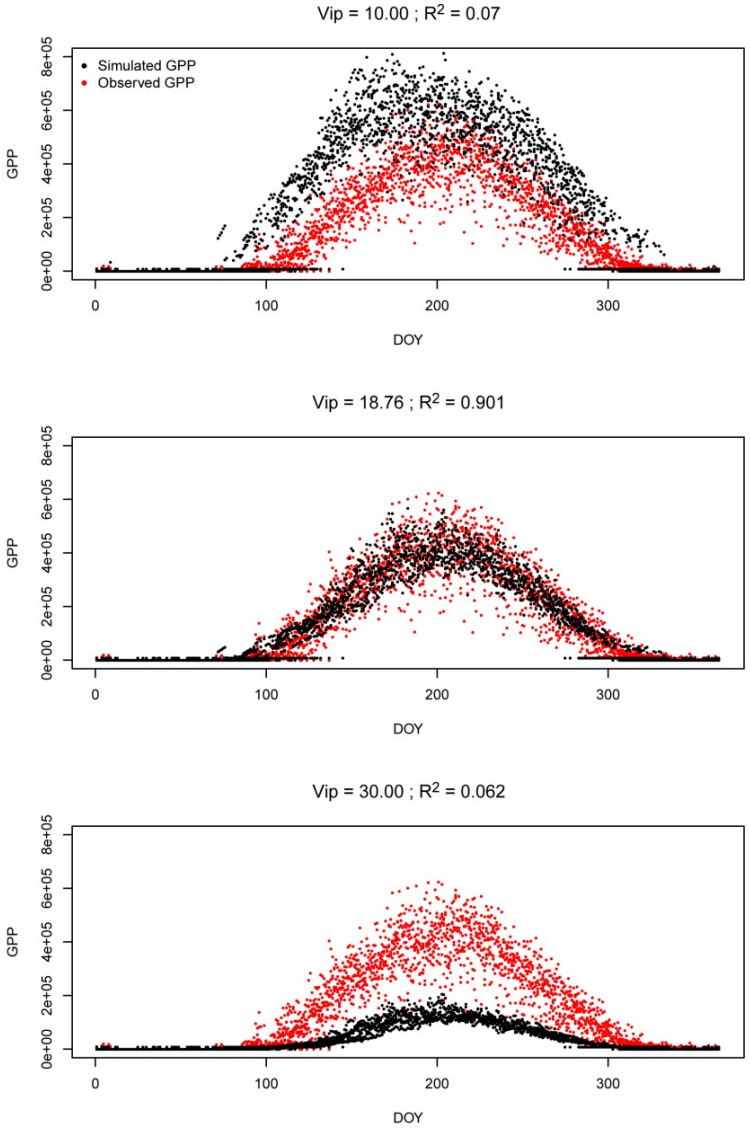

Figure S16: Sensitivity of the daily GPP simulated annual cycle (umol C m^{-2} day^{-1}) to the *Vip* parameter influencing $Vcmax$. Only *Vip* varies while the other parameters were fixed to the values of Plausible Block GPP. In the top (bottom) plot, *Vip* was fixed to the lowest (highest) value of its prior acceptable range. In the middle plot, it was fixed to the selected value for Plausible Block GPP. The R^2 between observations and simulations and the parameter value are reported for each plot.

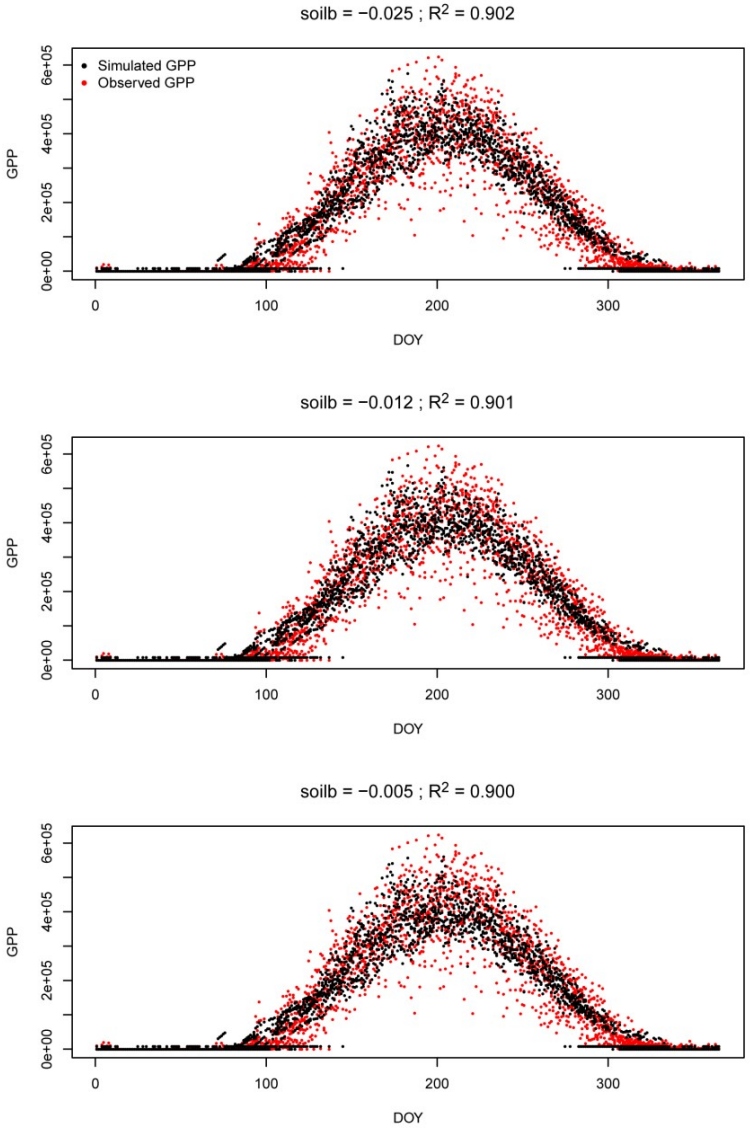

Figure S17: Sensitivity of the daily GPP simulated annual cycle (umol C m^{-2} day^{-1}) to the *soilb* parameter influencing θg.Only *soilb* varies while the other parameters were fixed to the values of Plausible Block GPP. In the top (bottom) plot, *soilb* was fixed to the lowest (highest) value of its prior acceptable range. In the middle plot, it was fixed to the selected value for Plausible Block GPP. The R^2 between observations and simulations and the parameter value are reported for each plot.

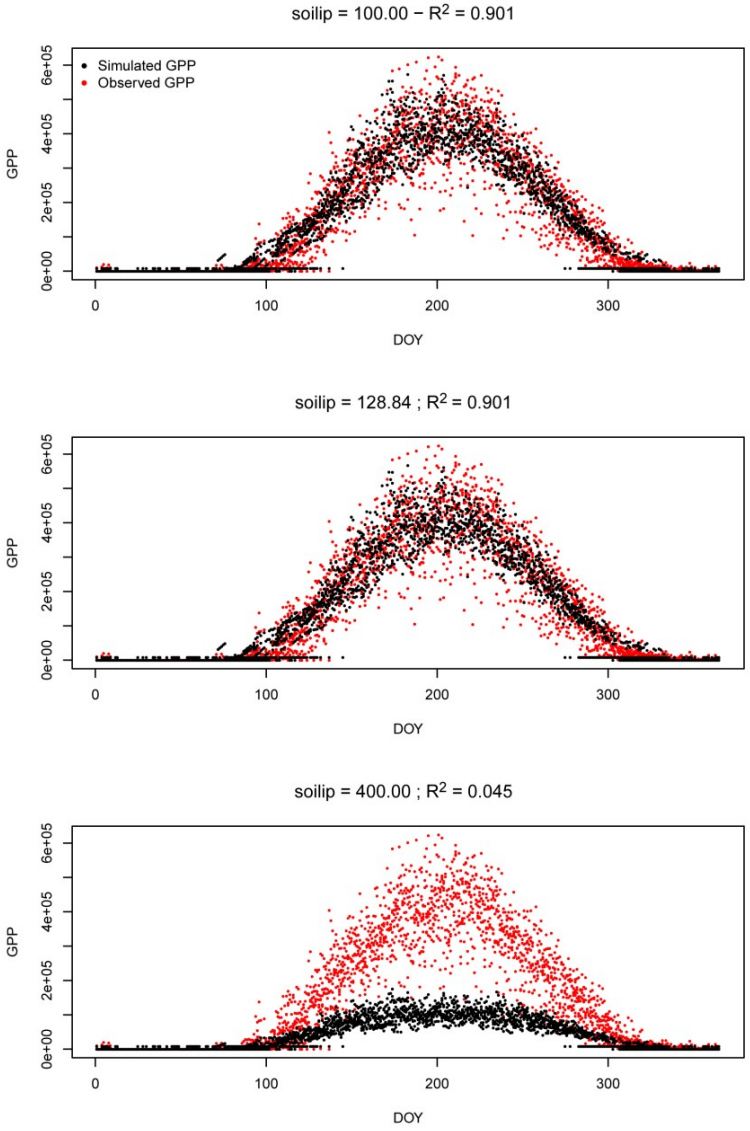

Figure S18: Sensitivity of the daily GPP simulated annual cycle (umol C m^{-2} day^{-1}) to the *soilip* parameter influencing θg. Only *soilip* varies while the other parameters were fixed to the values of Plausible Block GPP. In the top (bottom) plot, *soilip* was fixed to the lowest (highest) value of its prior acceptable range. In the middle plot, it was fixed to the selected value for Plausible Block GPP. The R^2 between observations and simulations and the parameter value are reported for each plot.

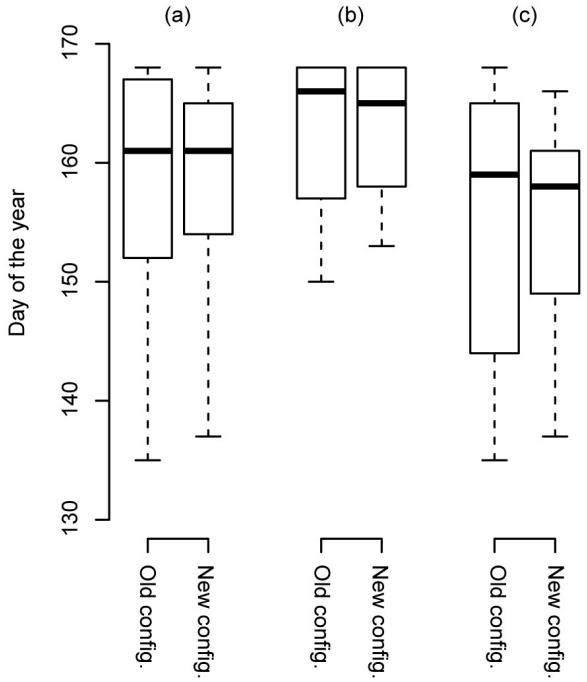

Figure S19: Growing season start (quartiles and extreme values) during the 1950-2010 (a), 1950-1970 (b) and 1990-2010 (c) periods. The parameters of Plausible Block Stem are used with ("New config."; *day23_flex* is set to 2) or without ("Old config."; *day23_flex* is set to 1 and has no effect) the mechanism to have more smoothed yearly variations.

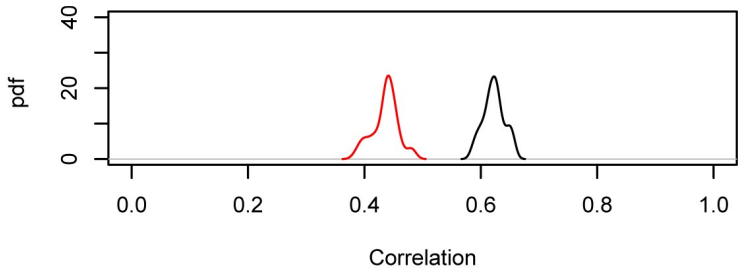

Figure S20: Impact of stored non-structural carbohydrates used in phase 3 (parameter *Cbud*) on the correlations between the mean of the detrended series of black spruce ring growth (RWhighF) and simulated yearly detrended C allocation to the stem. The pdfs are based on the 50 simulations retained by the Bayesian optimization. In black we see the results when the simulations use the optimized *Cbud* (see Fig. S8), in red when *Cbud* is set to 0 g C•m^{-2} of stand•day^{-1} (i.e. the stored carbon of the current and of the previous years is never remobilized).

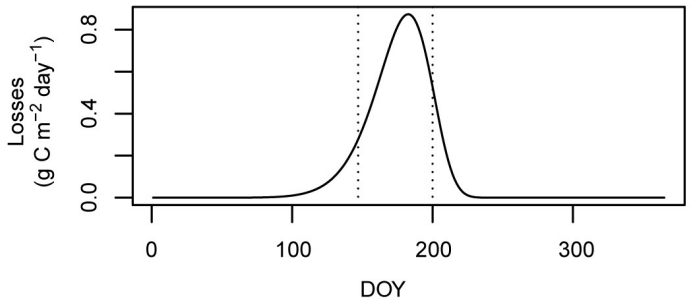

Figure S21: Simulated annual cycle of carbon losses from the canopy (i.e. leaf shedding) when MAIDEN runs with the parameters of Plausible Block Stem and the potential maximum amount of carbon that the canopy can contain during the year is 307 g C m^{-2} of stand (this value is the average of the simulated *AlloCcanopy*$_j$ values). Vertical dashed lines show the period over which the 80% of the yearly losses are observed.

Table S1: Cross-correlation analysis of the six parameters influencing the GPP. Correlations based on 50 retained blocks of parameters. Correlations with p < 0.01 are in bold.

	Vmax	*Vb*	*Vip*	*soilb*	*soilip*
Vb	**0.94**				
Vip	**0.99**	**0.97**			
soilb	-0.04	-0.10	-0.10		
soilip	0.36	0.15	0.25	0.10	
τ	0.08	0.21	0.11	-0.05	-0.23

Table S2: Cross-correlation analysis of the 12 parameters controlling the carbon allocation to the stem. Correlations based on 50 retained blocks of parameters. Correlations with p < 0.01 are in bold.

	CanopyT	*CanopyP*	*GDD1*	*vegphase23*	*day23_flex*	*Cbud*	*h3*	*st4temp*	*photoper*	*PercentFall*	*OutMax*
CanopyP	-0.18										
GDD1	0.01	0.18									
vegphase23	-0.07	0.13	**0.59**								
day23_flex	0.02	0.07	**0.50**	**0.39**							
Cbud	-0.05	-0.14	-0.23	-0.13	-0.27						
h3	0.17	-0.18	-0.21	-0.22	-0.23	-0.17					
st4temp	-0.09	0.08	-0.14	0.01	-0.14	0.09	0.12				
photoper	0.08	-0.02	-0.08	-0.05	0.22	-0.33	-0.17	**-0.40**			
PercentFall	-0.04	0.08	0.08	0.10	-0.04	**-0.49**	0.06	0.24	-0.10		
OutMax	-0.06	-0.21	-0.08	0.16	0.02	0.03	0.00	0.15	0.12	-0.09	
OutLength	-0.19	-0.05	-0.08	-0.12	-0.02	**0.47**	-0.20	-0.06	-0.16	0.00	0.32